Int. J. Solids Structures Vol. 26, No. 4, pp. 417–435, 1990
Printed in Great Britain.

0020-7683/90 $3.00 + .00

A MODEL FOR THE MECHANICAL STRESSES INDUCED BY HEAD–DISK CONTACT

J. J. KEREMES and G. B. SINCLAIR
Department of Mechanical Engineering, Carnegie Mellon University, Pittsburgh, PA 15213, U.S.A.

(*Received* 9 *August* 1988; *in revised form* 31 *March* 1989)

Abstract—A model is developed for the mechanical stresses resulting from contact between a flying head and a thin-film "rigid" disk of a magnetic storage system. The complexity of the configuration leads to a number of simplifying assumptions so as to render the problem tractable. In particular, the disk is treated as being comprised of homogeneous, isotropic, elastic layers; the normal loading is considered to be quasi-static provided dynamic enhancement is included; the tangential loads are simply taken to be the normal loading times a coefficient of friction; and the surface roughness is modelled as being sinusoidal in two dimensions. Even so, the problem is three-dimensional and geometrically nonlinear. Analysis proceeds on substructuring the model into a global problem for contact over the lowermost head planform and a local problem for asperity contact within this planform, with attention being focused on the latter. For the local problem, solutions for the contact stresses are obtained via an adaptation of the recent paper by Johnson *et al.* (1985, *Int. J. Mech. Sci.* **27**, 383), while solutions for the interior stresses are derived in closed form using Papkovich Neuber potentials. Some typical results are presented. In a full treatment of a system, these would have to be combined with the *in situ* and thermal stresses involved. Thus the present analysis simply provides a means for determining the mechanical contribution to the complete stress fields.

1. INTRODUCTION

Wear is a limiting factor in performance in many instances in engineering. One such case occurs in magnetic read/write systems used in the computer industry. Currently, some of these systems feature a magnetic recording head that floats on an air bearing a mere few hundred nanometers above a rotating, layered, hard or "rigid" disk on which information is both stored and retrieved in the form of magnetic fields. Improved recording performance could be obtained by shrinking the present distance between the head and the disk to an even smaller value. Unfortunately this is largely prohibited by the wear problem which results from the increased intermittent contact between the head and the disk. Such contact can degrade a disk to the point of catastrophic memory failure. It is therefore in the interests of the manufacturer to design a more robust system, both for safeguarding the stored information in current systems, and for lowering flying heights to improve the performance of new systems. Although this problem is a relative newcomer in tribology compared to such traditional problems as piston ring or bearing wear, it is nonetheless already approaching comparable monetary importance to these well-known wear problems.

Wear rates in thin-film rigid disk systems can be expected to be related to the stresses they experience, with configurations that have lower tensile and shear stresses relative to limiting values enjoying better performance. Accordingly, here we seek to begin to gain an understanding of the stresses induced in a disk on contact with a head. These fields are comprised of *in situ* stresses and thermomechanical operating stresses. As a start, we consider the latter, specifically the mechanical stresses. Ultimately such stresses need to be combined with both their *in situ* and thermal counterparts for a full appreciation of the stress fields produced. Moreover, in this assembling some interaction can occur. For example, as Barber (1969) points out, the temperature elevation caused by friction heating can lead to thermal distortions which in turn alter contact areas and change mechanical stresses. Our intent, then, is to furnish a means for sufficiently realistic estimation of the mechanical stress contribution to eventually enable this analysis to be effective when used as one element of the necessarily iterative process of determining the complete stress fields within a disk.

Even confining attention to the mechanical contact stresses in a disk, the problem is complex. Consequently we need to employ a number of simplifying assumptions. First, we

view the disk as being comprised of *linear elastic, homogeneous and isotropic*, layers. The use of a continuum approach is justified since, while some of the layers involved are very thin, they are still at least two orders of magnitude larger than atomic spacings. The use of elasticity is largely justified by our primary concern with the operating stresses that occur after any burnishing or planishing and hence after the bulk of any permanent deformation—eventually the stresses accrued in operations like burnishing need to be incorporated with the intrinsic stresses of formation to provide the *in situ* stresses. The assumption of homogeneity and isotropism within each layer is probably less justified since the volumes of material of interest may well be too small to admit to the usual averaging of such features as microvoid distributions, grain orientations, etc. However, at present, it would seem to be difficult to obtain reliable physical characterizations of these aspects, so that increasing the complexity of our model by attempting to accommodate local inhomogeneities/anisotropy is probably an activity that better awaits greater assurance that the companion physical measurements are available. In contrast, estimates of the pairs of elastic moduli required for each layer can be made so that we can recognize the stratified heterogeneity of the disk, a feature which is important since certainly the thin protective overcoats often used are quite comparable to the size of the contact regions.

Second, we model the disk surface as having a *sinusoidal waviness* in *two dimensions*, while taking subsurface *interfaces* as being *perfectly bonded* and *flat*, for the following reasons. Although disk and head surfaces are finished so as to be extremely smooth, asperity contact does occur in practice and can result in real areas of contact that are as much as two orders of magnitude smaller than apparent areas. Such effects cannot be ignored. Further, there is the possibility of interactions between neighboring asperities and contact at each asperity produces subsurface stresses with marked three-dimensional aspects.† Modelling the disk surface as having sinusoidal profiles in two orthogonal directions allows us to capture this pair of effects, as well as enabling the introduction of some anisotropy in surface roughness through the selection of different wavelengths in the two directions. By choosing the amplitude of the surface waves to reflect the combined roughness of the disk and the head we can approximate the latter as being flat—in essence this is applying Hertz's assumptions to heterogeneous media. Notice though, that the wavelengths and amplitudes of a surface's roughness are, in fact, randomly distributed. Thus a simulation drawing on their distributions is really required to determine associated mean or representative stress values for comparing different disk configurations. At this time, the hope is that, by picking a representative surface roughness, we can obtain representative companion stresses from a single analysis without undertaking a simulation involving multiple analyses. Ultimately this needs to be checked. Consequently, although we do not undertake this extensive exercise here, we do have as a further objective that any model developed should be sufficiently computationally attractive so as to enable its repeated application in whatever future simulations are found necessary. Turning to the interfaces between layers, we assume they are perfectly bonded because this is certainly the intent in their manufacture and the alternative is probably too complex to merit investigation at this stage.‡ Given perfect bonding, any small deviations from being perfectly flat can be consistently ignored by a further application of Hertz's assumption in effect.

Third, we take the loading to be *quasi-static* with the *shear* contribution given by applied *normal* tractions *times a friction coefficient*: the rationale for these last assumptions is given below. In justification of the quasi-static simplification, we note that the relative

† By way of an example of such three-dimensional effects, consider the smooth Hertzian contact of a sphere on an elastic half-space wherein one two-dimensional idealization would be to replace the sphere with an infinitely long cylinder. The three-dimensional problem has a radial tensile stress at the edge of the contact region of magnitude $\bar{p}(1-2\nu)/2$ where $\bar{p}$ is the average pressure and ν is Poisson's ratio. The two-dimensional problem has stresses that are nowhere tensile throughout the upper surface. While the magnitude of the tensile stress in the 3D problem is not great, since any tensile stresses can be important in making inferences about failure mechanisms this sort of difference is potentially quite significant.

‡ In this connection we remark that imperfectly bonded layers imply interface cracks, thus a fracture mechanics approach with considerably more effort required in its necessarily detailed analysis as well as difficult physical measurements to quantify flaw distribution and critical values for crack propagation.

speed between the disk and the head is such that the contact time can be expected to be around two orders of magnitude greater than the time it takes for elastic waves to travel through the near field of interest. Hence averaging occurs and the same stresses should result from a quasi-static analysis as a full elastodynamic one provided the applied loading is increased to reflect momentum losses—in essence this is Love's criterion for being able to employ a quasi-static approach. Finally, regarding the applied shear, we observe that friction forces are found to be comparable to normal in practice and consequently need to be included, while simply assuming a Coulomb law of sliding friction holds point by point for the actual tractions is *in lieu* of anything obviously clearly superior that entails a similar degree of difficulty.

The determination of mechanical stresses under the above conditions constitutes a contact problem within mechanics. There is an extensive literature on this class of problems—see Kalker (1977a) for a fairly recent review. Focusing on elastic response which includes the effects of a wavy surface, probably the first contribution is that by Westergaard (1939). In Westergaard's paper, the contact between two slightly wavy surfaces, whose gap distance is described by a cosine curve, is treated as a plane strain problem for the homogeneous half-space. A closed form solution is produced for the contact pressure and area. This same problem is considered independently by Dundurs *et al.* (1973) and by Kuznetsov (1982). The more difficult three-dimensional contact between surfaces with two-dimensional waviness has apparently only recently been investigated for a homogeneous half-space by Johnson *et al.* (1985). The geometric nonlinearity of the changing contact shape is the key difficulty in this problem which is solved numerically. These papers focus on the contact stresses and provide information only in the absence of friction and for homogeneous wavy bodies. Contributions which include friction and/or involve layered half-spaces, on the other hand, do not include the effects of multiple surface asperities. Perhaps the most relevant examples of such work are: Hamilton and Goodman (1966), Dhaliwal and Rau (1970), Chen and Engel (1972), and O'Sullivan and King (1986). In Hamilton and Goodman's paper, the quasi-static solution for a sliding spherical indenter in contact with a homogeneous half-space is developed, including explicit interior response. In Dhaliwal and Rau's paper, the effects of inhomogeneity caused by a single layer, under frictionless contact, are examined. In Chen and Engel's paper, frictionless contact with up to two layers on top of a half-space is studied; this paper also presents an extensive review of the literature for similar problems (through 1970). In O'Sullivan and King's report, the same contact problem as considered by Dhaliwal and Rau is investigated, but with friction included and with the main emphasis on the interior response. Needed for present purposes therefore is an analysis which incorporates the effects of surface waviness, friction, and a layered subsurface. Our intention is to furnish such a treatment.

We begin in Section 2 by discussing the model formulation, continue in Section 3 with the method of solution (some details of which are appended), and close in Section 4 with selected results and some discussion.

2. MODEL FORMULATION

Here we provide problem statements for our model. In order to considerably reduce the effort involved in subsequent analysis, we substructure the determination of the mechanical stresses in a disk into the solution of a *global problem* then a *local problem*. The global problem addresses the nominal surface tractions induced by contact over the entire bottom plane of the head: the local problem then seeks the redistributed surface and interior stresses in the disk resulting from asperity contact with the gross contact area (Fig. 1). In addition, in view of our basic objective of determining *representative* mechanical stresses that ultimately enable *comparison* of the complete stress fields for different configurations, it probably suffices to largely limit the scope of the present work to local aspects. The rationale for this focusing is as below. Given in some sense an optimum shaped head from a stress point of view, the maximum of the normal gross contact stress takes on its minimum value of $\bar{p}$, the average pressure. Alternatively, with smooth Hertzian contact over a flat elliptical planform, the maximum is only $3\bar{p}/2$. Thus provided "sharp" corners are avoided at the edges of the

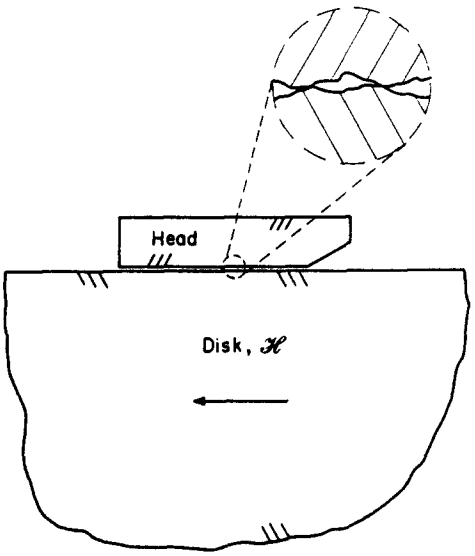

Fig. 1. Global and local head–disk contact.

head's bottom surface, the peak gross pressure can be expected to be bounded within a fairly narrow range. Moreover, the gross pressure really represents the *loading* on an asperity, and changing loads produce relatively minor changes in local contact stresses because, as the load increases, the local area over which it acts increases, and vice versa.† Turning then to the local problem, we further subdivide our approach by considering it to be formed by the superposition of a normal loading problem and a tangential counterpart. The formulation of these two key problems follows.

We let $\mathscr{H}$ denote the half-space and take x_i $(i = 1, 2, 3)$ to be rectangular Cartesian coordinates with origin O such that the x_1x_2 plane through O forms the surface of $\mathscr{H}$ with x_3 positive into $\mathscr{H}$, i.e.

$$\mathscr{H} = \{(x_1, x_2, x_3) \,|\, |x_1| < \infty, |x_2| < \infty, 0 < x_3 < \infty\}. \tag{1}$$

Assuming periodic loading of $\mathscr{H}$ with periods $2L_1$, $2L_2$ in the x_1, x_2 directions respectively, attention can be confined to a representative cell comprised of N layers, $\mathscr{C}_n$ $(n = 1, 2, \ldots, N)$, with the last layer being semi-infinite (Fig. 2).‡ That is

$$\mathscr{C}_n = \{(x_1, x_2, x_3) \,|\, |x_1| < L_1, |x_2| < L_2, D_{n-1} < x_3 < D_n\}, \tag{2}$$

wherein D_n is the depth to the bottom of the nth layer with the understanding that $D_0 = 0$, $D_N = \infty$. The upper surfaces of the layers are

$$\partial\mathscr{C}_n = \{(x_1, x_2, x_3) \,|\, |x_1| < L_1, |x_2| < L_2, x_3 = D_{n-1}\}. \tag{3}$$

Thus for $n = 2, 3, \ldots, N$ these are the layer interfaces while for $n = 1$ we obtain the upper surface of the cell. For this upper surface, we model the total waviness of the head and disk as creating a gap, G, given by

$$G = (\Delta/4)[2 - \cos(\pi x_1/L_1) - \cos(\pi x_2/L_2)], \tag{4}$$

where Δ is representative of the amplitude of the combined roughness of the head and disk. Further, we partition this surface into a contact area, $\partial\mathscr{C}_c$, and a free surface, $\partial\mathscr{C}_f$, with

† For example, in the Hertzian contact of a smooth sphere the contact stresses are proportional to load to the power 1/3.

‡ The index n is reserved solely for layer identification and takes the values $1, 2, \ldots, N$, while the indices i, j, k range over 1, 2, 3.

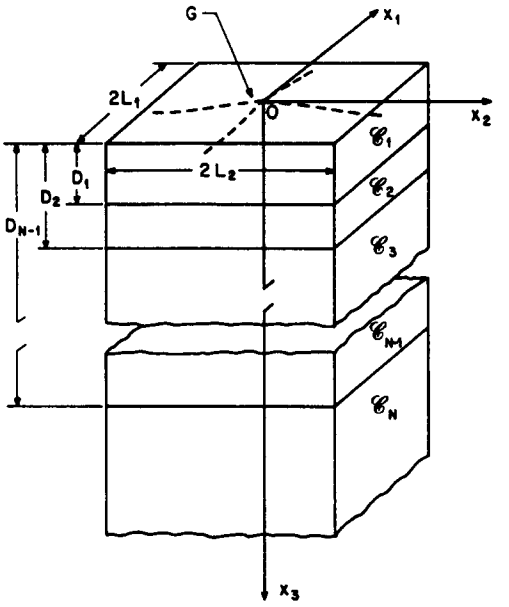

Fig. 2. Geometry and coordinates for the layered cell.

$$\partial\mathscr{C}_c = \{(x_1, x_2, x_3) \mid |x_1| < R\cos\theta,\ |x_2| < R\sin\theta,\ x_3 = 0\},$$
$$\partial\mathscr{C}_c \cup \partial\mathscr{C}_f = \partial\mathscr{C}_1, \quad \partial\mathscr{C}_c \cap \partial\mathscr{C}_f = \varnothing, \tag{5}$$

wherein $R = R(\theta)$ $(0 \leqslant \theta < 2\pi)$ defines the extent of the contact region and $\varnothing$ is the null set. With these geometric preliminaries in place, we can now state our local model problem for the disk response under normal contact loading.

We seek the *periodic* stress components σ_{ij} and displacements u_i as functions of x_i throughout all $\mathscr{C}_n$, together with the extent of the local contact region R and the maximum depth of indentation δ, subject to the following. The stress *equations of equilibrium*, in the absence of body forces under the assumption of quasi-static response,

$$\sigma_{ij,j} = 0, \tag{6}$$

on $\mathscr{C}_n$.† The *stress–displacement relations* for each homogeneous and isotropic, linear elastic layer,

$$\sigma_{ij} = \mu_n\left[\left(\frac{2\nu_n}{1-2\nu_n}\right)u_{k,k}\delta_{ij} + u_{i,j} + u_{j,i}\right], \tag{7}$$

on $\mathscr{C}_n$, where μ_n, ν_n are respectively the shear modulus and Poisson's ratio of $\mathscr{C}_n$, and δ_{ij} is the Kronecker delta. The *contact conditions* which redistribute an applied, nominal, average pressure, p, so that a perfectly smooth flat surface indents the wavy upper surface of the half-space cell to a maximum depth of δ, viz.

$$u_3 = \delta - G, \quad \sigma_{31} = \sigma_{32} = 0, \tag{8}$$

on $\partial\mathscr{C}_c$, with

† The usual index notation conventions apply; repeated i, j, k subscripts imply summation and a subscript preceded by a comma indicates partial differentiation with respect to the corresponding Cartesian coordinate.

$$\int_{\partial\mathscr{C}_c} \sigma_{33}\,dx_1\,dx_2 = -4pL_1L_2 (p > 0). \tag{9}$$

The *stress-free conditions* for the remainder of the upper surface of the cell,

$$\sigma_{3i} = 0, \tag{10}$$

on $\partial\mathscr{C}_f$. The *interface conditions* for perfect bonding between the layers,

$$u_i^+ = u_i^-, \quad \sigma_{3i}^+ = \sigma_{3i}^-, \tag{11}$$

on $\partial\mathscr{C}_n$ $(n \neq 1)$, where plus denotes the limit as $x_3 \to D_n$ with $x_3 > D_n$, and minus is the same limit but with $x_3 < D_n$. The *conditions at infinity*, which reflect the net nominal loading,

$$\sigma_{33} = -p + o(1), \quad \sigma_{31} = o(1), \quad \sigma_{32} = o(1) \text{ as } x_3 \to \infty, \tag{12}$$

on $\mathscr{C}_N$. The *symmetry conditions* resulting from the periodic loading,

$$\begin{aligned} &u_1 = 0, \quad \sigma_{12} = \sigma_{31} = 0 \text{ at } |x_1| = L_1 (|x_2| < L_2, 0 < x_3 < \infty), \\ &u_2 = 0, \quad \sigma_{12} = \sigma_{23} = 0 \text{ at } |x_2| = L_2 (|x_1| < L_1, 0 < x_3 < \infty). \end{aligned} \tag{13}$$

And, adjoining all the foregoing equations, the *contact inequalities* which ensure no tensile tractions are transmitted within the contact region and no interpenetration of the head and disk surfaces outside the contact region.† That is,

$$\sigma_{33} \leqslant 0 \text{ on } \partial\mathscr{C}_c, \quad u_3 \geqslant \delta - G \text{ on } \partial\mathscr{C}_f. \tag{14}$$

Several comments concerning the foregoing are in order. First, a disk is usually comprised of a thin protective overcoat, a magnetic storage layer of comparable thickness, and one or two substrates that are typically two or more orders of magnitude thicker than either upper layer. Thus since bending stresses right through the disk are not significant in the vicinity of the contact region (the bending moment being zero there), it is reasonable to treat the bottom layer as semi-infinite relative to the uppermost layers of greatest interest. Further, N is typically not more than 4 and, if in fact there are two thick lower substrates, can be reduced to 3 or even 2 without unduly affecting the key stress fields if two or more of these layers have comparable elastic moduli. Second, it is not obvious how to choose Δ of (4) to model surface roughness. However, provided a consistent basis is chosen, such as the combined root-mean-square variation of the disk and head surfaces, it would seem possible to obtain sufficiently representative stress values to enable comparisons. Third, the treating of the indenting surface as rigid is an approximation. This approximation is exact for a homogeneous half-space and indenter provided the modulus of the idented material is adjusted in the determination of the contact stresses. By taking effective moduli for the disk and head, a similar adjustment in the contact stress evaluation can be made here and we can expect no great errors from this simplification. Fourth, the assumption of a perfectly smooth or frictionless indenter is temporary—we remove it next by merely applying shear tractions that are point by point the same as the normal in the above multiplied by a coefficient of friction. In introducing friction in this way, we are ignoring any effects it might have on the contact area—for coefficients that are typically of the order of one half or less, this is probably a reasonable approximation. The friction problem statement then is as follows.

† These inequalities are necessary to make the smooth Hertzian contact of a rigid sphere on an elastic half-space a well-posed problem, so we can expect them to apply here.

We seek additional periodic stresses σ_{ij} and displacements u_i as functions of x_i throughout all $\mathscr{C}_n$ subject to the following. The *field equations*, (6), (7). The *friction contact conditions*, for relative motion in the x_1 direction,

$$\sigma_{31} = f\bar{\sigma}_{33}, \quad \sigma_{23} = \sigma_{33} = 0, \tag{15}$$

on $\partial\mathscr{C}_c$, where f is the coefficient of friction, constant on $\partial\mathscr{C}_c$, and the bar on σ_{33} is reserved for this surface component on $\partial\mathscr{C}_c$ drawn from the normal contact loading problem. The *stress-free conditions*, (10). The *interface conditions*, (11). The *conditions at infinity* which reflect the net tangential loading,

$$\sigma_{31} = -fp + o(1), \quad \sigma_{32} = o(1), \quad \sigma_{33} = o(1) \text{ as } x_3 \to \infty, \tag{16}$$

on $\mathscr{C}_\infty$. Finally, the *symmetry/antisymmetry conditions* resulting from the periodic loading, namely (13) with the first equation therein replaced with

$$u_2 = u_3 = 0, \quad \sigma_{11} = 0 \text{ at } |x_1| = L_1 (|x_2| < L_2, 0 < x_3 < \infty). \tag{17}$$

Equation (17) concludes our formulation of the two local model problems of major interest.

3. ANALYSIS

In this section we first consider the local contact stresses at asperities in the normal loading problem, drawing on analyses in the literature. Next we construct potentials to recover the attendant interior response. Thereafter we treat the friction problem: herein the contact stresses are immediate from the normal loading problem while the interior response can be determined by an adaptation of the same.

Prior to commencing the analysis we adopt the following simplification. Since the actual results ultimately presented here do not include any anisotropy of surface roughness, we take advantage of the fact to set, from henceforth,

$$L_1 = L_2 = L, \tag{18}$$

wherein L is the common half-period of surface waviness. We do indicate, though, how the analysis would proceed in the event $L_1 \neq L_2$.

Turning to the literature as it relates to the determination of the *contact stress* and *region* in the *first problem* formulated in Section 2, we begin with Johnson *et al.* (1985). In Johnson *et al.*, a solution is developed for the contact region and pressure within it when a smooth flat indenter is pressed into a homogeneous elastic half-space with a two-dimensional wavy surface similar to that in (4). In general this is not a simple problem because the contact region cannot be specified *a priori*: Johnson *et al.* employ a numerical analysis of an equivalent variational statement (due to Kalker, 1977b) to estimate contact regions and stresses which are then checked experimentally. However, as noted in Johnson *et al.*, the contact region and pressure are asymptotic to those of isolated Hertzian contact provided the loads are sufficiently light. More precisely, if p^* is the applied average pressure for complete contact, then Hertzian conditions at the surface are effectively realized when

$$p/p^* \lesssim 0.1. \tag{19}$$

Herein

$$p^* = \pi E^* \Delta / 4L, \tag{20}$$

where E^* is a modified elastic modulus adjusted so as to reflect the deformation of the indenter as well as that of the half-space (see Johnson *et al.*, 1985, p. 384). For the smoothness and loading levels typically experienced in magnetic recording systems, we can anticipate (19) to be complied with. Thus if a disk were to be comprised of a single material,

the contact radius, R, would be nearly constant ($\not\propto \theta$), and the contact stress for the wavy surface, σ^{w}_{33}, would be well approximated by

$$\sigma^{w}_{33} \doteq \sigma^{h}_{33} = -\frac{6pL^2}{\pi R^2}\sqrt{1-(r/R)^2}, \tag{21}$$

where σ^{h}_{33} is the Hertzian stress for isolated contact on a homogeneous half-space and $r = \sqrt{(x_1^2+x_2^2)}$. As our disk is not homogeneous, we next look for a means of modifying the above to account for its heterogeneity.

Given that the wavy surface problem behaves like an array of isolated contacts, at least so far as the contact regions and pressures are concerned, one means of gauging the effects of heterogeneity is to consider a single parabolic identer acting on a layered half-space. Here the axisymmetry maintains R as a constant. This enables the usual inverse approach to be taken, namely choosing R then backing out the loading or applied average pressure necessary to achieve it [provided any such p does not lead to a violation of (19)]. Then our estimate of the contact stress $\bar{\sigma}_{33}$, for the normal loading problem is simply

$$\bar{\sigma}_{33} \doteq \sigma^{l}_{33}, \tag{22}$$

wherein σ^{l}_{33} is the contact stress for the layered half-space. For the disks of interest here, the greatest difference in moduli can be expected to occur between the protective overcoat and the other deeper layers, so that a two-layer half-space should suffice so far as the determination of the contact stress is concerned.† One estimate of σ^{l}_{33} for a two-layer half-space can be obtained from Dhaliwal and Rau (1970), which has

$$\sigma^{l}_{33} = \frac{-2}{\pi R^2}\int_r^R \frac{\Phi(\xi)}{\sqrt{\xi^2-r^2}}\,\mathrm{d}\xi, \tag{23}$$

in which ξ is the variable of integration and Φ is an unknown function which can be found from a Fredholm integral equation of the second kind [eqn (3.15) of Dhaliwal and Rau, 1970]. The numerical solution of this integral equation and ensuing integration to form σ^{l}_{33} are routine—see Keremes and Sinclair (1987a) for a description of a code to this end.

The foregoing estimation of $\bar{\sigma}_{33}$ is limited but has the virtue of simplicity. An increase in its range of applicability (up to p/p^* of about 0.2) may be obtained merely by fitting the Johnson *et al.* results to furnish an estimate of σ^{w}_{33} somewhat different from σ^{h}_{33}, then taking

$$\bar{\sigma}_{33} \doteq \sigma^{w}_{33}(\sigma^{l}_{33}/\sigma^{h}_{33}). \tag{24}$$

Now σ^{l}_{33}, σ^{h}_{33} act over slightly perturbed values of R as θ varies and have to be adjusted accordingly. At higher load levels, interaction between waviness and heterogeneity can be expected so that (24) ceases to approximate well. In such cases, extension of Johnson *et al.* (1985) to include the effects of a layered half-space could be considered, albeit at the expense of some effort. At this time, we confine our attention to configurations complying with (19), and merely use (22), (23) to obtain the contact stress in the normal loading problem.

To find the companion *interior responses*, we first seek an elementary stress field that renders the conditions at infinity homogeneous: this aids in determining the remaining fields and can also reveal some basic facets of the interior solution. Construction is straightforward. We take $\sigma_{33} = -p$ to make (12) homogeneous, and thereafter adjust the constant magnitude of the other normal stress components so that the corresponding strains are zero. Then satisfaction of equilibrium, (6), is automatic, and integration of (7) yields u_3 on $\mathscr{C}_n$ as the only existing displacement so that the symmetry conditions, (13), hold. On

† For configurations that have other marked differences in moduli, more layers may need to be considered: the analysis of Chen and Engel (1972) should prove useful in such circumstances.

selecting the constants of integration on each $\mathscr{C}_n$ such that the matching conditions, (11), are met, the end result is

$$\sigma_{33} = -p, \quad \sigma_{11} = \sigma_{22} = -p\nu_n/(1-\nu_n),$$
$$u_3 = -p\gamma_n x_3 + p\sum_{n'=1}^{n} D_{n'-1}(\gamma_{n'} - \gamma_{n'-1}), \quad \gamma_n = \frac{1-2\nu_n}{2\mu_n(1-\nu_n)}, \tag{25}$$

on $\mathscr{C}_n$ with all other stresses and displacements being zero, where γ_n is the material constant indicated with the understanding $\gamma_0 = 1$ (recall $D_0 = 0$), and n' is a dummy layer index.† Interesting to note is that, while under (19) the contact stresses do not really feel neighboring contact points, the transverse stresses of (25) demonstrate that the interior stresses can be sensitive to neighbors. This is especially so since the magnitudes of the transverse pressures in (25) can be expected to be comparable to any tensile stresses in this region, and thus may even completely negate them. The residual fields that complement (25) must now satisfy

$$\sigma_{3i} = o(1) \text{ as } x_3 \to \infty, \tag{26}$$

on $\mathscr{C}_N$, as well as

$$\sigma_{33} = \bar{\sigma}'_{33}, \quad \sigma_{23} = \sigma_{31} = 0, \tag{27}$$

on $\partial\mathscr{C}_1$, where

$$\bar{\sigma}'_{33} = \bar{\sigma}_{33} + p \text{ on } \partial\mathscr{C}_c, \quad \bar{\sigma}'_{33} = p \text{ on } \partial\mathscr{C}_f, \tag{28}$$

with $\bar{\sigma}_{33}$ being our solution for the normal contact stress. We assemble these next.

For the residual fields, we look to Papkovich Neuber potentials since these reduce satisfaction of the three-dimensional field equations to the determination of up to four harmonic functions, and in the present periodic context these functions can be expected to admit separable solutions in terms of elementary functions. Thus we take

$$u_i = \frac{1}{2\mu_n}[\phi_{,i} + x_j\psi_{j,i} - \kappa_n\psi_i], \tag{29}$$

on $\mathscr{C}_n$, where ϕ, ψ_i are the harmonic potentials ensuring (6), (7) hold and κ_n is the material constant defined by

$$\kappa_n = 3 - 4\nu_n. \tag{30}$$

The separable solutions required for any periodic normal loading of a homogeneous half-space can be found in, for example, Fung (1965, p. 195), and only entail ϕ and ψ_3. For our layered cell, we simply use these forms, distinguishing the constants involved by layer, to arrive at

$$\begin{Bmatrix} \psi_3 \\ \phi \end{Bmatrix} = \left[\begin{Bmatrix} a_n \\ b_n \end{Bmatrix} e^{-\beta_{ml}x_3} + \begin{Bmatrix} c_n \\ d_n \end{Bmatrix} e^{\beta_{ml}x_3} \right] \cos \alpha_m x_1 \cos \alpha_l x_2, \tag{31}$$

on $\mathscr{C}_n$. In (31), a_n, b_n, c_n, d_n are constants on $\mathscr{C}_n$, and

† Observe that these fields give rise to unbounded displacements as $x_3 \to \infty$. Thus the periodic problem, with its infinite total loading of the entire surface of the half-space, shares the indeterminancy of *two-dimensional* contact problems. That is, while the extent the "indenter" penetrates into and contacts with the substrate, as well as the associated stresses, are unique, the actual displacement of the identer remains undetermined.

$$\alpha_m = m\pi L, \quad \alpha_l = l\pi L, \quad \beta_{ml} = \sqrt{(\alpha_m^2 + \alpha_l^2)}, \tag{32}$$

where m, l are eigenvalue indices ($m, l = 0, 1, 2, \ldots, \infty$).† The corresponding eigenvalue displacements, $\hat{u}_i$, and stresses, $\hat{\sigma}_{ij}$ are directly obtained from (29), (7):

$$\begin{Bmatrix} \hat{u}_1 \\ \hat{u}_2 \end{Bmatrix} = \frac{-1}{2\mu_n}[(a_n x_3 + b_n)\, e^{-\beta_{ml} x_3} + (c_n x_3 + d_n)\, e^{\beta_{ml} x_3}] \begin{Bmatrix} \alpha_m \sin \alpha_m x_1 \cos \alpha_l x_2 \\ \alpha_l \cos \alpha_m x_1 \sin \alpha_l x_2 \end{Bmatrix},$$

$$\hat{u}_3 = \frac{-1}{2\mu_n}[(a_n(\kappa_n + \beta_{ml} x_3) + b_n \beta_{ml})\, e^{-\beta_{ml} x_3} + (c_n(\kappa_n - \beta_{ml} x_3) - d_n \beta_{ml})\, e^{\beta_{ml} x_3}] \cos \alpha_m x_1 \cos \alpha_l x_2, \tag{33}$$

on $\mathscr{C}_n$, and

$$\begin{Bmatrix} \hat{\sigma}_{11} \\ \hat{\sigma}_{22} \end{Bmatrix} = \left[\left(2a_n \nu_n \beta_{ml} - (a_n x_3 + b_n) \begin{Bmatrix} \alpha_m^2 \\ \alpha_l^2 \end{Bmatrix} \right) e^{-\beta_{ml} x_3} - \left(2c_n \nu_n \beta_{ml} + (c_n x_3 + d_n) \begin{Bmatrix} \alpha_m^2 \\ \alpha_l^2 \end{Bmatrix} \right) e^{\beta_{ml} x_3} \right] \cos \alpha_m x_1 \cos \alpha_l x_2, \tag{34}$$

$$\hat{\sigma}_{33} = 2(a_n e^{-\beta_{ml} x_3} - c_n e^{\beta_{ml} x_3})(1 + \nu_n)\beta_{ml} \cos \alpha_m x_1 \cos \alpha_l x_2 - \hat{\sigma}_{11} - \hat{\sigma}_{22},$$

$$\hat{\sigma}_{12} = [(a_n x_3 + b_n)\, e^{-\beta_{ml} x_3} + (c_n x_3 + d_n)\, e^{\beta_{ml} x_3}] \alpha_m \alpha_l \sin \alpha_m x_1 \sin \alpha_l x_2,$$

$$\begin{Bmatrix} \hat{\sigma}_{23} \\ \hat{\sigma}_{31} \end{Bmatrix} = [(a_n(1 - 2\nu_n + \beta_{ml} x_3) + b_n \beta_{ml})\, e^{-\beta_{ml} x_3} + (c_n(1 - 2\nu_n - \beta_{ml} x_3) - d_n \beta_{ml})\, e^{\beta_{ml} x_3}] \begin{Bmatrix} \alpha_l \cos \alpha_m x_1 \sin \alpha_l x_2 \\ \alpha_m \sin \alpha_m x_1 \cos \alpha_l x_2 \end{Bmatrix},$$

on $\mathscr{C}_n$. In addition to satisfying the field equations, (6), (7), these displacements and stresses meet the symmetry requirements, (13). Moreover, to ensure satisfaction of their infinity conditions, (26), we merely exclude $m = l = 0$ and set

$$c_N = d_N = 0. \tag{35}$$

It remains to adjust the other constants in (33), (34) so that the matching conditions, (11), and surface conditions, (27), (28), are complied with.

For the matching conditions, substituting (33), (34) into the six requirements on $\partial\mathscr{C}_n$ in (11) reduces them to four independent conditions because $\hat{u}_2$ is automatically matched once $\hat{u}_1$ is, as is $\hat{\sigma}_{31}$ once $\hat{\sigma}_{23}$ is. Consequently the resulting system has a 4×4 matrix, with elements evaluated on $\mathscr{C}_n$, premultiplying the vector of unknown constants, $\mathbf{a}_n = (a_n, b_n, c_n, d_n)$, and set equal to a similar 4×4 matrix, with elements evaluated on $\mathscr{C}_{n+1}$, premultiplying the vector $\mathbf{a}_{n+1}$. Forming the inverse of the first matrix and premultiplying through by it yields

$$\mathbf{a}_n = \mathbf{T}_n \mathbf{a}_{n+1}, \tag{36}$$

wherein $\mathbf{T}_n$ is the transfer matrix enabling the constants in $\mathscr{C}_n$ to be expressed in terms of those in $\mathscr{C}_{n+1}$. Straightforward but tedious algebra furnishes the elements of $\mathbf{T}_n$ which are given in the Appendix. Successively applying (36) allows the constants in any layer to be expressed in terms of those in the last semi-infinite layer and fulfills the matching condition on all $\mathscr{C}_n$ ($n \neq 1$). That is,

† It is appropriate at this point to note changes for instances when $L_1 \neq L_2$. These are: in (21) replace L^2 by $L_1 L_2$ and in (32) α_m, α_l become $m\pi/L_1$, $l\pi/L_2$, respectively.

$$\mathbf{a}_n = \left(\prod_{n'=n}^{N-1} \mathbf{T}_{n'}\right)\mathbf{a}_N, \tag{37}$$

for $n = 1, 2, \ldots, N-1$. In particular, $\mathbf{a}_1$ can thus be related to the two unknowns in $\mathbf{a}_N$, a_N and b_N [recall (35)].

To obtain two further conditions for the determination of the constants, we look to the surface requirements. With a view to satisfying the normal stress requirement in (27), (28) via a summation of eigenfunctions, we normalize the coefficient of the trigonometric functions in $\hat{\sigma}_{33}$ on $\partial\mathscr{C}_1$ to obtain one condition. Thereafter, enforcing the first shear stress requirement in (27) furnishes a second, viz.

$$\begin{aligned} 2(a_1 - c_1)(1 - \nu_1)\beta_{ml} + (b_1 + d_1)\beta_{ml}^2 &= 1, \\ (a_1 + c_1)(1 - 2\nu_1) + (b_1 - d_1)\beta_{ml} &= 0, \end{aligned} \tag{38}$$

provided $m^2 + l^2 \neq 0$. As earlier, the second shear stress requirement in (27) is automatically met. Now on expressing $\mathbf{a}_1$ in terms of a_N, b_N, the entire set of constants for any one multilayered eigenfunction can be found using (37) and (38). Summing such eigenfunctions and meeting the actual normal stress requirement in (27), (28) gives the fields for the residual problem as being

$$\sigma_{ij} = \sum_{m=0}^{\infty}\sum_{l=0}^{\infty} A_{ml}\hat{\sigma}_{ij}, \quad u_i = \sum_{m=0}^{\infty}\sum_{l=0}^{\infty} A_{ml}\hat{u}_i, \tag{39}$$

where $m^2 + l^2 \neq 0$ and

$$A_{ml} = \frac{2k_{ml}}{L^2}\int_0^L \int_0^L \bar{\sigma}'_{33} \cos \alpha_m x_1 \cos \alpha_l x_2 \, dx_1 \, dx_2, \tag{40}$$

with $k_{ml} = 1$ if $ml = 0$, $k_{ml} = 2$ otherwise. If we now adopt the understanding that when $m = l = 0$ the fields in (39) are to be supplemented by those of (25), we have a complete solution for the interior response in the first, normal loading, contact problem. For a specific configuration, the evaluation of this solution proceeds routinely on performing the necessary matrix multiplication and numerical quadrature provided some care is exercised to control round-off errors in the exponential terms in the former activity—Keremes and Sinclair (1987b) provides details of a code to this end.

Turning to the *friction problem*, the contact stresses are immediate in the light of (15), (22), while the interior response can be found in a similar manner to that for the normal loading problem. In somewhat greater detail, we first remove elementary elastic fields that maintain the symmetry/antisymmetry conditions in (13), (17) while rendering the infinity conditions, (16), homogeneous. The construction of such fields parallels the earlier effort and yields

$$\sigma_{31} = -fp, \quad u_1 = -fp\left[\frac{x_3}{\mu_n} - \sum_{n'=1}^{n} D_{n'-1}\left(\frac{1}{\mu_{n'}} - \frac{1}{\mu_{n'-1}}\right)\right], \tag{41}$$

on $\mathscr{C}_n$, with all other stresses and displacements being zero and $\mu_0 = 1$ (recall $D_0 = 0$). For the residual problem, the Papkovich Neuber potentials are not readily available in the literature but after some thought can be shown to be

$$\begin{Bmatrix}\psi_1\\ \psi_2\end{Bmatrix} = -[a_n e^{-\beta_{ml}x_3} + d_n e^{\beta_{ml}x_3}] \begin{Bmatrix}\alpha_l \cos \alpha_m x_1 \cos \alpha_l x_2\\ \alpha_m \sin \alpha_m x_1 \sin \alpha_l x_2\end{Bmatrix},$$

$$\begin{Bmatrix}\psi_3\\ \psi'_3\end{Bmatrix} = \left[\begin{Bmatrix}b_n\\ c_n\end{Bmatrix} e^{-\beta_{ml}x_3} + \begin{Bmatrix}e_n\\ f_n\end{Bmatrix} e^{\beta_{ml}x_3}\right] \sin \alpha_m x_1 \cos \alpha_l x_2,$$

$$\phi = -x_1\psi_1 - x_2\psi_2 + \psi'_3, \tag{42}$$

on $\mathscr{C}_n$, where ψ'_3 is an auxiliary potential introduced solely to compact the equations. The forms in (42) merit a little discussion. The functions associated with b_n, c_n, e_n and f_n are the obvious shear counterparts of (31), and provide four independent constants per layer. Now, though, the six matching conditions in (11) do not collapse to four so that two further constants are needed. These are generated by considering x_1 and x_2 multipliers of harmonic functions in ϕ and adjusting the coefficients of these products so that, in combination, they are harmonic. In this way ϕ gives rise to some further displacements and stresses that are of the same functional form as the initial obvious ones, together with some unwanted different forms. These last are removed with ψ_1 and ψ_2 to arrive at the potentials in (42). The displacements and stresses associated with (42) are furnished in the Appendix. Provided d_N, e_N and f_N are set to zero, they satisfy all the requirements except the matching and surface. Complying with these follows the approach used in the normal loading problem, except that now the transfer matrix $\mathbf{T}'_n$, is 6×6, and the surface requirements lead to three equations.† Finally, summing eigenfunctions and adjoining (41) completes the solution of the friction problem and our analysis here (details of the evaluation procedures for specific configurations can again be found in Keremes and Sinclair, 1987b).

4. RESULTS AND DISCUSSION

In this section we first present results with a view to verifying the preceding analysis, then the stress distributions for a baseline configuration. Thereafter we examine in turn the effects on peak tensile and shear stresses of changes in: the applied average pressure, the coefficient of friction, the surface roughness, the thickness of the uppermost layer or overcoat, and the modulus of the overcoat.

As our initial *check problem*, we consider the *homogeneous* half-space indented on a small circle $R = L/5$. This is within the range wherein the wavy surface problem is locally axisymmetric, so that, in the near field, our normal loading solution should reproduce the Hertz solution, while our friction solution should recover its shear counterpart derived in Hamilton and Goodman (1966). Comparing σ_{33} on the x_3 axis for the periodic, normal, loading problem with that for the Hertz problem (from Hamilton and Goodman), we find agreement within 1% of the maximum contact stress at the origin, O, for $0 \leqslant x_3 \leqslant 10R$. Deeper within the half-space, σ_{33} for the periodic loading approaches the average applied pressure on a cell, p, while σ_{33} for the Hertz loading decays to zero. Comparing σ_{13} on the x_3 axis for the periodic friction problem with that for the shear Hertz problem (from Hamilton and Goodman), we find agreement within 1% of the stress at O for $0 \leqslant x_3 \leqslant R/2$. The more restrictive range here is because the decay to the respective far-field values, namely $-fp$ (f being the coefficient of friction) and zero, is far more rapid than for the normal loading problem. The good agreement found is to be expected since the series solutions developed in Section 3 enjoy transcendental convergence in the interior: hence the foregoing comparisons really just serve as a check on the coding in Keremes and Sinclair (1987a, b). A more rigorous test is at the surface where there are no exponential terms to assist the convergence: here, provided sufficient eigenfunctions are included, good agreement is maintained except near the edges of the contact region where the stress fields are not continuously differentiable. Since our solution can be compared directly with prescribed values in boundary conditions in this instance, a fuller examination of its accuracy can await a situation which activates more of its features. Accordingly we look to carry out

† The elements of $\mathbf{T}'_n$ are given in the Appendix.

Table 1. Specifications for the baseline configuration

Loading	Geometry	Moduli
$p_0 = 170$ (kPa)	$(D_1)_0 = 0.035$ (μm)	$(\mu_1)_0 = 200 \times 10^3$ (MPa)
$f_0 = 0.2$	$(D_2)_0 = \infty$	$(\mu_1/\mu_2)_0 = 5/2$
	$L_0 = 50\Delta_0 = 5$ (μm)	$(\nu_1)_0 = 5(\nu_2)_0/6 = 1.4$

such a check on a configuration that is more typical of that encountered in magnetic recording.

The defining values for our typical or *baseline configuration* are set out in Table 1; these and other values associated with this configuration are distinguished by the added subscript zero. The entries in Table 1 are not intended to be specific to any one system, merely typical of a class of thin-film rigid disks. Nonetheless their selection bears some comment. Regarding the loading, the light spring force in the suspension system for the head, when acting over the gross area of the head that is available for contact, can produce a nominal pressure of 10–20 kPa. Dynamic enhancement of nominal loads can increase them by a factor of two in a number of simple structural systems, and by 10^2 or more for impact loading such as occurs when a weight is dropped on a substrate. Here, somewhat arbitrarily, we take a factor of about 10. The friction contribution is assigned a coefficient of 0.2, probably rather on the low side of the coefficients measured in practice—subsequently we consider a higher value. In justification of the geometry, we observe that a number of manufacturers employ a protective overcoat of, say, a diamond-like-carbon (DLC), overlying a magnetic layer of, for example, nickel–cobalt, on top of a base substrate of nickel–phosphorus, which in turn rests on an aluminum base. The overcoat is of the order of 200–500 Å thick [thus $(D_1)_0$], the magnetic layer is about twice as thick, the base substrate two orders of magnitude thicker, and the Al base thicker still. Since the shear moduli of the Ni–Co and Ni–P layers only differ by around 10%, they can be treated as one. Further, the difference in moduli between the aluminum base and the nickel layers is not felt in the near field because it occurs at a remote location, in terms of multiples a way of characterizing distances such as overcoat thickness, contact extent, etc. Accordingly, for the mechanical stresses in such disks, we can treat all the layers beneath the overcoat as one [hence $(D_2)_0$].† Turning to the surface, profile measurements indicate that the combined roughness of the head and the disk can be up to about three times the thickness of the overcoat, while peak-to-peak distances are of the order of 100 times the peak amplitudes (thus L_0, Δ_0). Finally concerning elastic properties, the shear modulus of the DLC can be expected to lie between the extremes of the high value of diamond and the low value of graphite—somewhat arbitrarily within the range we take a value of 200 MPa. This leads to a shear modulus for the nickel-type layer of 40% of that of the overcoat. We take Poisson's ratios of 0.25, 0.3 for the first, second layers respectively because these are reasonable values which do include a minor difference.

Now as our *second check*, we examine how well the *surface conditions*, (8), (10), (14) are complied with for the normal loading in our baseline configuration. Taking the specifications from Table 1, we find that the contact radius is well within the locally axisymmetric regime with $R = 0.026L$. Consequently, since the shear stress requirements in (8), (10) hold exactly for our solution, it remains to confirm the displacement condition inside the contact circle and the stress-free condition for the normal component outside. We can anticipate the greatest convergence difficulties lying in the satisfaction of the latter. This is because the derivatives of the stress field are not continuous at the edge of the contact region, indeed are not even piecewise continuous. This can be shown to give rise to stresses with a limiting convergence rate of $O(m^{-3/2})$ as $m \to \infty$ [alternatively $O(l^{-3/2})$ as $l \to \infty$]. The displacements on the other hand, being integrals of the stresses, have a limiting

† Several calculations including the Al base as a distinct layer demonstrated that the near-field stresses remained the same within 5%, confirming that two layers suffice here. On the other hand, no attempt at this time has been made to include any super thin layers introduced to aid adhesion between the overcoat and the magnetic layer: provided such layers were no less than about $(D_1)_0/10$ thick, a three-layer version of the present analysis could probably model them.

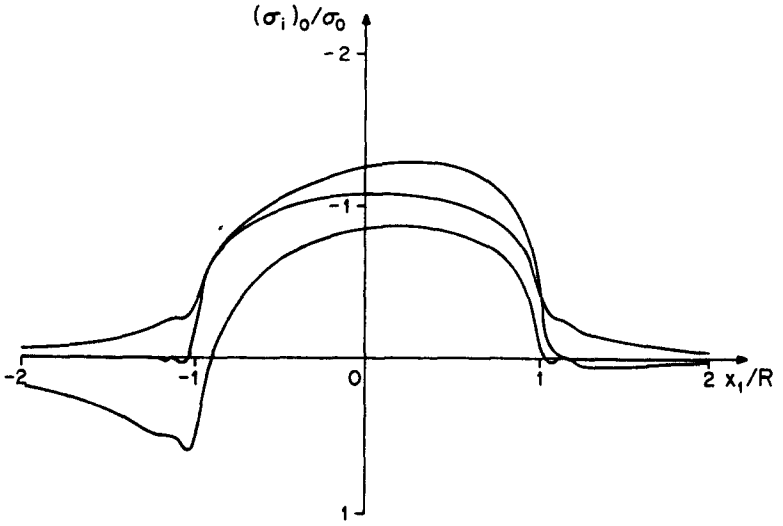

Fig. 3. Principal surface stresses for the baseline configuration ($x_2 = x_3 = 0$).

convergence rate of $O(m^{-5/2})$ as $m \to \infty$. As a result we proceed as follows: we successively double m and l until the minimum number of eigenfunctions, $(m+1)(l+1)-1$, is found such that adequate agreement with the normal stress requirement is obtained. In this way we find that with $m = l = 64$, or 4,224 eigenfunctions, the maximum error occurs just outside the contact circle, at $r = 1.05R$, as the solution attempts to drive the contact pressure to zero. Here it overshoots by 3% of the contact pressure at the origin. Subsequent oscillations in the normal stress decrease in amplitude as r increases till they become negligible at stations with $r \geqslant 1.2R$. In the interests of keeping computational effort down, we deem this adequate agreement.† In addition, the stresses within the contact region are everywhere compressive in accordance with (14). For this number of eigenfunctions, the displacements throughout the contact region agree with prescribed values to within 1/2% of the central displacement. Such improved accuracy is in line with convergence expectations. Further, outside the contact region, the displacements do not interpenetrate the flat indenting surface in accordance with (14). All the surface conditions for the normal loading problem are thus adequately met with m, l being truncated at 64, and we use the associated number of eigenfunctions henceforth.‡

As a *last check*, we examine whether the surface conditions (10), (15) hold for the *friction* loading in our baseline problem. Here we find a similar error distribution in σ_{31} to that in σ_{33} for the normal loading problem, but now the maximum error as a percentage of the *normal* stress at the origin for the *combined* problems is a factor of five smaller because of the lower applied shear stresses (recall $f_0 = 0.2$). With this last satisfactory result, all the surface conditions in (8), (10), (14), (15) hold. Since the method of construction ensures analytical compliance with the field equations and other conditions, this completes the verification of our solution.

Selected *results for the baseline configuration* are shown in Figs 3, 4, 5. These display principal stresses, $(\sigma_i)_0$, normalized by σ_0, where σ_0 is defined by

$$\sigma_0 = \sigma_{33} \text{ at O for the baseline configuration.§} \tag{43}$$

How the principal stresses vary with x_1/R along the x_1 axis at the surface and at the interface is shown in Figs 3 and 4, respectively: Fig. 5 shows the variation with x_3/R down the x_3

† Computation time for the baseline configuration with this number of eigenfunctions was quite reasonable, being less than 30 min on a time-sharing VAX 3000.

‡ In passing we remark that the same number of eigenfunctions is used in the first check problem.

§ Note that the actual σ_0 here is 480 MPa, so that yielding would not seem to be a foregone conclusion, especially since the fields are predominantly all-round compression (in the Hertz problem, this compressive nature means σ_0 has to reach about 5/3 times the uniaxial yield stress for the onset of subsurface yielding).

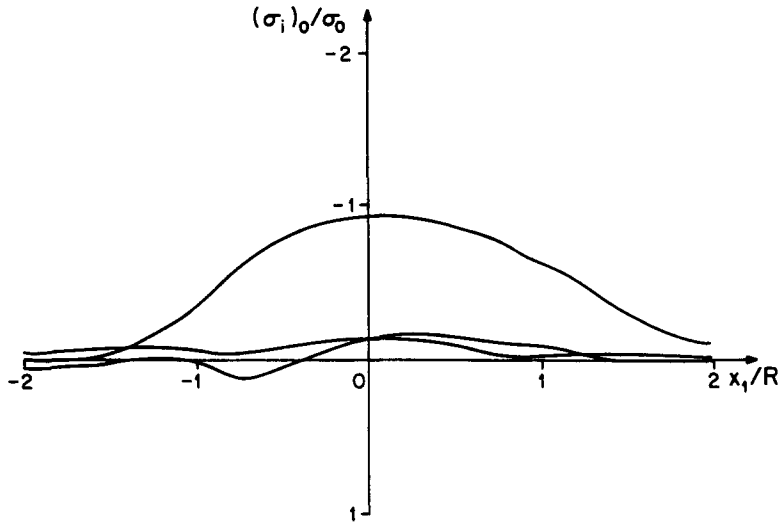

Fig. 4. Principal interface stresses for the baseline configuration [$x_2 = 0$, $x_3 = (D_1)_0$].

axis. Some discussion of these figures is appropriate. In Fig.3, one of the principal stresses coincides with σ_{33} outside the contact region, and thus illustrates the sort of errors encountered in satisfaction of the stress-free requirement. The lack of symmetry about $x_1/R = 0$ is due to the friction present: accordingly, since the dominant tensile stress is quite antisymmetric, a significant contribution to this stress must stem from the friction loading. The maximum shear occurs in the vicinity of this tensile stress, namely near the edge of the contact region on the left side, so that this location is a prime one for surface failure. In Fig. 4, the stresses on the interface show markedly reduced magnitudes except for the major compressive component. Again the antisymmetry is due to friction which can therefore be credited with a significant contribution to what little tensile stress there is on the interface

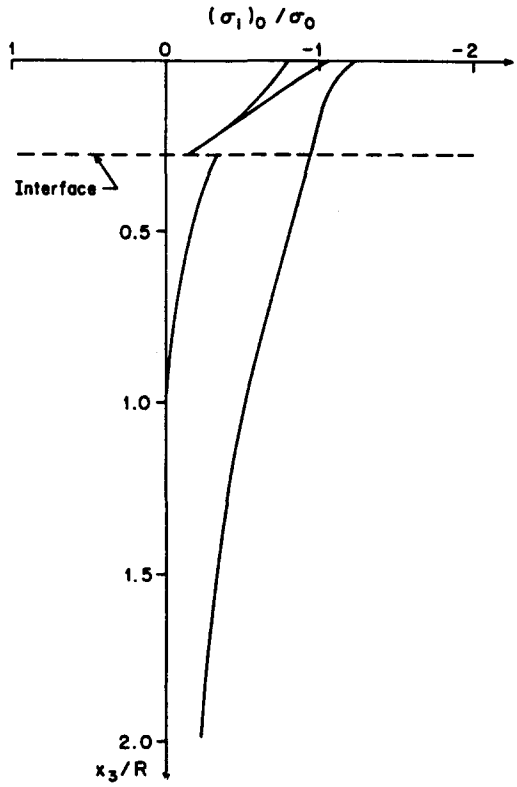

Fig. 5. Principal stresses down the x_3 axis for the baseline configuration.

Table 2. Effects of different configurations on key stresses

Case number	Distinctive feature	Maximum surface tensile stress ($/\sigma_0$)	Maximum surface shear stress ($/\sigma_0$)	Maximum interface tensile stress ($/\sigma_0$)	Maximum interface shear stress ($/\sigma_0$)
0	—	0.61	0.44	0.11	0.42
1	$p = \frac{1}{2}p_0$	0.46	0.34	0.10	0.37
2	$p = 2p_0$	0.81	0.57	0.13	0.51
3	$f = 3f_0$	1.39	0.81	0.39	0.52
4	$\frac{\Delta}{L} = \frac{1}{2}\left(\frac{\Delta}{L}\right)_0$	0.43	0.28	0.12	0.21
5	$\frac{\Delta}{L} = 2\left(\frac{\Delta}{L}\right)_0$	0.86	0.69	0.54	0.85
6	$D_1 = \frac{1}{2}(D_1)_0$	0.66	0.44	0.15	0.35
7	$D_1 = 2(D_1)_0$	0.55	0.44	0.27	0.55
8	$\mu_1 = \frac{1}{3}(\mu_1)_0$	0.38	0.25	0.05	0.29
9	$\mu_1 = 2(\mu_1)_0$	0.80	0.68	0.49	0.67

(occurring under the edge of the contact region). Now, though, the maximum shear has moved to a station close to directly under the center of the contacted area above. In Fig. 5, there is a change of scale for the x_3/R coordinate, cf. x_1/R in Figs 1, 2. This is because the stresses have already started to behave predictably at $x_3/R \geqslant 2$, conforming to the asymptotic behavior of components from isolated periodic contact on a homogeneous half-space [as in eqs (9), (15) of Hamilton and Goodman (1966) when combined with (25), (41)]. Within the overcoat, the transverse normal stresses are nearly equal and can be approximated as the sum of a uniform compressive field plus a pure bending field: the latter is due to the overcoat being stiffer than the substrate and acting like a plate on soft springs under transverse loading. At the bottom of the overcoat, while continuity of the normal stress acting on the interface is required, it is not for normal stresses acting parallel to it, and indeed Fig. 5 shows that these stresses are discontinuous. In all of these figures, the effects of asperity–asperity interaction are negligible. The main attribute of our periodic solution in this instance lies in its facilitating an analytical solution, which in turn aids in parameter studies.† Further results for this and other configurations are given in Keremes and Sinclair (1987c); we review some of the results for other configurations next.

Distinguished by case number in Table 2, the *variations about the baseline configuration* (Case 0) seek to examine, in order, the effects of: decreases and increases in applied average pressure (Cases 1, 2), a larger coefficient of friction (Case 3), smoother and rougher upper surfaces (Cases 4, 5), thinner and thicker overcoats (Cases 6, 7), and softer and stiffer overcoats (Cases 8, 9). In every instance, only the aspect indicated is changed, and the effects are summarized in terms of maximum tensile and shear stresses at the surface and the interface, all of which are normalized by σ_0 of (43). While these stresses are by no means the only ones affecting failure, they are important in this regard and serve to indicate trends when various aspects of head–disk contact are altered.

The *varying applied average pressures* entertained in Table 2 probably represent the extremes that could be achieved by contouring or a lack of contouring of an otherwise smooth head, free from sharp corners and edges.‡ Even with these extremes, the effects are limited, being felt most at the surface where on average stresses go down by 24% when p is halved, and go up by 31% when p is doubled. In fact these surfaces stresses show very much the same dependence on loading as noted earlier in Section 2, being proportional to

† This absence of asperity–asperity interaction need not always be so. If the present analysis is used up to the limit of its extended range of applicability, $p/p^* = 0.2$, then transverse compressive stresses like those of (25) can nullify up to 40% of the tensile stresses occurring at the interface.

‡ See Paparizos and Sinclair (1989).

$p^{1/3}$. In all, the gross applied pressure would not seem to be a critical feature for the mechanical stresses in head–disk contact under most circumstances.

The *increase* in the coefficient of *friction* to 0.6 in Table 2 is within measured values and produces a pronounced effect. It more than doubles the maximum tension at the surface while tripling this stress at the interface, thereby reinforcing the earlier observation of its role in this respect. Also, it almost doubles the maximum surface shear, but has relatively little effect on the interface shear. In sum friction effects can be very significant in determining the mechanical stresses due to head–disk contact.

The somewhat arbitrarily chosen *smoother* and *rougher surfaces* in Table 2 also produce marked changes. The smoother finish lowers the surface stresses by, on average, 33%, and halves the maximum interface shear. The rougher finish increases the surface stresses by, on average, 49%, and more than doubles both interface stresses. The overall sensitivity here is every bit as high as that for variations in friction coefficient. In all, the surface roughness would appear to be a key factor for the mechanical stresses accompanying head–disk contact.

Finally, regarding the *overcoat*. The *changes* in *thickness* in Table 2 probably are approaching the limits set in practice by the need to produce a consistent thickness (D_1 being halved), and the objective that the separation between the magnetic fields in the head and the disk be minimal (D_1 being doubled). The *variations* in *shear modulus* in Table 2 reduce the overcoat stiffness to being the same as the substrate, and increase it to an upper bound which is somewhat in excess of even that for pure diamond. The effects of thickness changes are small. Reducing thickness typically increases stresses slightly, while increasing thickness reduces surface stresses yet increases interface stresses. The effects of modulus changes are far more marked. The less stiff overcoat uniformly reduces stresses by, on average, 42%, probably largely because of the removal of shear moduli mismatch. These results are within 3% of those for a completely homogeneous half-space, demonstrating the minor influence of differences in Poisson's ratios. The stiffer overcoat uniformly increases stresses with the surface stresses and interface shear increasing by, on average, 48%. The interface tensile stress is increased by more than a factor of 4 because of the greater bending occurring as the overcoat acts like a stiff covering plate. In sum, while changes in the overcoat thickness would not seem to play a major role in altering the mechanical stresses in head–disk contact, adjustments to the overcoat moduli quite conceivably could.

All of the preceding discussion focuses on the effects of various rearrangements of head–disk configurations on the mechanical stresses *alone*. At this time, it would therefore be quite premature to infer the effects of the changes considered on the complete stress fields, let alone on the wear performance. Perhaps a better interpretation of the sensitivity study summarized in Table 2 is that it identifies parameters that need to be carefully characterized if the mechanical stress contribution is to be sufficiently accurately captured. Specifically, the most critical parameters would seem to be the coefficient of friction, the surface roughness, and the overcoat modulus. Given reasonable representative values for these, together with estimates of the other parameters, the present mechanical stress analysis should suffice for inclusion in a complete stress analysis.

Acknowledgements—We are pleased to extend our thanks to Y.-T. Hsia, G. C. Rauch and R. E. Rottmayer of DEC for valuable comments received during the course of this study. The financial support of the Magnetics Technology Center at Carnegie Mellon University is also appreciated.

REFERENCES

Barber, J. R. (1969). Thermoelastic instabilities in the sliding of conforming solids. *Proc. R. Soc.* (*Lond.*) **A312**, 381.

Chen, W. T. and Engel, P. A. (1972). Impact and contact stress analysis in multilayered media. *Int. J. Solids Structures* **8**, 1257.

Dhaliwal, R. S. and Rau, I. S. (1970). The axisymmetric Boussinesq problem for a thick elastic layer under a punch of arbitrary profile. *Int. J. Engng Sci.* **8**, 843.

Dundurs, J., Tsai, K. C. and Keer, L. H. (1973). Contact between elastic bodies with wavy surfaces. *J. Elasticity* **3**, 109.

Fung, Y. C. (1965). *Foundations of Solid Mechanics*. Prentice-Hall, Englewood Cliffs, New Jersey.

Hamilton, G. M. and Goodman, L. E. (1966). The stress field created by a circular sliding contact. *J. Appl. Mech.* **33,** 371.
Johnson, K. L., Greenwood, J. A. and Higginson, J. G. (1985). The contact of elastic regular wavy surfaces. *Int. J. Mech. Sci.* **27,** 383.
Kalker, J. J. (1977a). A survey of the mechanics of contact between solid bodies. *Z. Angew. Math. Mech.* **57,** T3.
Kalker, J. J. (1977b). Variational principles of contact elastostatics. *J. Inst. Math. Applic.* **20,** 199.
Keremes, J. J. and Sinclair, G. B. (1987a). Documentation of PARPUNCH: a contact stress analysis code for a parabolic punch pushed into a layered elastic half-space. Report SM 87-13, Department of Mechanical Engineering, Carnegie Mellon University, Pittsburgh, PA
Keremes, J. J. and Sinclair, G. B. (1987b). Documentation of PERLAY: a stress analysis code for the periodically loaded, layered half-space. Report SM 87-8, Department of Mechanical Engineering, Carnegie Mellon University, Pittsburgh, PA
Keremes, J. J. and Sinclair, G. B. (1987c). Mechanical stress results for a variety of head/disk configurations. Report SM 87-12, Department of Mechanical Engineering, Carnegie Mellon University, Pittsburgh, PA.
Kuznetsov, Ye A. (1982). A periodic contact problem accounting for the additional load acting beyond the indenter (in Russian). *Izv. Acad. Nauk SSSR, Mekh. Tverd. Tela* **17,** 84.
O'Sullivan, T. C. and King, R. B. (1986). Sliding contact stress field due to a spherical indenter on a layered elastic half-space. IBM Research Report, RJ 5363 (55702).
Paparizos, L. G. and Sinclair, G. B. (1989). On contouring to reduce contact stresses. *Proc. Twelfth CANCAM*, Ottawa, Canada, **1,** 276.
Westergaard, H. M. (1939). Bearing pressures and cracks. *J. Appl. Mech.* **6,** 49.

APPENDIX

Here we furnish the algebraic details needed to complete the solutions developed in Section 3. First we give the elements of the *transfer matrix*, $\mathbf{T}_n$, for the *normal loading contact problem*:

$$\mathbf{T}_n = \left(\frac{t_{qs}}{4\mu_{n+1}(1-\nu_n)}\right).$$

where t_{qs} $(q, s = 1, 2, 3, 4)$ are given by:

$$t_{11} = t_{22} = \mu_{n+1}\kappa_n + \mu_n,$$
$$t_{33} = t_{44} = \mu_{n+1} + \mu_n\kappa_{n+1},$$
$$t_{31} = t_{42} = 0,$$
$$t_{12} = -\bar{\mu}_n(\kappa_n + 2\beta_{ml}D_n)\,e^{2\beta_{ml}D_n},$$
$$t_{13} = [\bar{\mu}_n(1-2\nu_n)(\kappa_{n+1} + 2\beta_{ml}D_n) - 2\bar{\nu}_n(\mu_{n+1} - 2\mu_n\beta_{ml}D_n)]\beta_{ml}^{-1},$$
$$t_{14} = [\bar{\mu}_n(\kappa_{n+1}(1-2\nu_n) - 2\beta_{ml}^2D_n^2) - 2\bar{\nu}_n(\mu_{n+1} + 2\bar{\mu}_n\beta_{ml}D_n)]\beta_{ml}^{-1}\,e^{2\beta_{ml}D_n},$$
$$t_{32} = 2\bar{\mu}_n\beta_{ml}\,e^{2\beta_{ml}D_n},$$
$$t_{34} = -\bar{\mu}_n(\kappa_{n+1} - 2\beta_{ml}D_n)\,e^{2\beta_{ml}D_n},$$

with the remainder of the elements given by changing the sign of D_n in accordance with

$$t_{21} = \bar{\mu}_n(\kappa_n - 2\beta_{ml}D_n)\,e^{-2\beta_{ml}D_n} = t_{12}(-D_n),$$
$$t_{23} = -t_{14}(-D_n), \quad t_{24} = -t_{13}(-D_n),$$
$$t_{41} = -t_{32}(-D_n), \quad t_{43} = t_{34}(-D_n).$$

In the above, $m^2 + l^2 \neq 0$ and

$$\bar{\mu}_n = \mu_{n+1} - \mu_n, \quad \bar{\nu}_n = \nu_{n+1} - \nu_n,$$

so it follows immediately that, if $\mu_{n+1} = \mu_n$, $\nu_{n+1} = \nu_n$, then $\mathbf{T}_n$ becomes the unit matrix as it should. Next we provide the forms for the *displacements* and *stresses* in the *friction* or *shear loading problem*:

$$\begin{Bmatrix}\hat{u}_1\\ \hat{u}_2\end{Bmatrix} = \frac{1}{2\mu_n}\left[\left(4a_n(1-\nu_n)\left(\frac{\alpha_l}{\alpha_m}\right)\begin{Bmatrix}1\\-1\end{Bmatrix} + (b_nx_3 + c_n)\begin{Bmatrix}1\\-1\end{Bmatrix}\right)e^{-\beta_{ml}x_3}\right.$$
$$\left. + \left(4d_n(1-\nu_n)\left(\frac{\alpha_l}{\alpha_m}\right)\begin{Bmatrix}1\\-1\end{Bmatrix} + (e_nx_3 + f_n)\begin{Bmatrix}1\\-1\end{Bmatrix}\right)e^{\beta_{ml}x_3}\right]\begin{Bmatrix}\alpha_m\cos\alpha_mx_1\cos\alpha_lx_2\\ \alpha_l\sin\alpha_mx_1\sin\alpha_lx_2\end{Bmatrix},$$

$$\hat{u}_3 = \frac{-1}{2\mu_n}[(b_n(\kappa_n + \beta_{ml}x_3) + c_n\beta_{ml})\,e^{-\beta_{ml}x_3} + (e_n(\kappa_n - \beta_{ml}x_3) - f_n\beta_{ml})\,e^{\beta_{ml}x_3}]\sin\alpha_mx_1\cos\alpha_lx_2.$$

$$\begin{Bmatrix}\hat{\sigma}_{11}\\ \hat{\sigma}_{22}\end{Bmatrix} = -\left[\left(4a_n(1-\nu_n)\alpha_m\alpha_l\begin{Bmatrix}1\\-1\end{Bmatrix} - 2b_n\nu_n\beta_{ml} + (b_n x_3 + c_n)\begin{Bmatrix}\alpha_m^2\\ \alpha_l^2\end{Bmatrix}\right)e^{-\beta_{ml}x_3}\right.$$
$$\left. + \left(4d_n(1-\nu_n)\alpha_m\alpha_l\begin{Bmatrix}1\\-1\end{Bmatrix} + 2e_n\nu_n\beta_{ml} + (e_n x_3 + f_n)\begin{Bmatrix}\alpha_m^2\\ \alpha_l^2\end{Bmatrix}\right)e^{\beta_{ml}x_3}\right]\sin\alpha_m x_1\cos\alpha_l x_2,$$

$$\hat{\sigma}_{33} = 2(b_n e^{-\beta_{ml}x_3} - e_n e^{\beta_{ml}x_3})(1+\nu_n)\beta_{ml}\sin\alpha_m x_1\cos\alpha_l x_2 - \hat{\sigma}_{11} - \hat{\sigma}_{22},$$

$$\hat{\sigma}_{12} = [(2a_n(1-\nu_n)(\alpha_m^2-\alpha_l^2) - (b_n x_3 + c_n)\alpha_m\alpha_l)\,e^{-\beta_{ml}x_3}$$
$$+ (2d_n(1-\nu_n)(\alpha_m^2-\alpha_l^2) - (e_n x_3 + f_n)\alpha_m\alpha_l)\,e^{\beta_{ml}x_3}]\cos\alpha_m x_1\sin\alpha_l x_2,$$

$$\begin{Bmatrix}\hat{\sigma}_{23}\\ \hat{\sigma}_{31}\end{Bmatrix} = \left[\left(-2a_n(1-\nu_n)\beta_{ml}\left(\frac{\alpha_m}{\alpha_l}\right)\begin{Bmatrix}1\\-1\end{Bmatrix} + (b_n(1-2\nu_n+\beta_{ml}x_3)\right.\right.$$
$$\left. + c_n\beta_{ml})\begin{Bmatrix}1\\-1\end{Bmatrix}\right)e^{-\beta_{ml}x_3} + \left(2d_n(1-\nu_n)\beta_{ml}\left(\frac{\alpha_m}{\alpha_l}\right)\begin{Bmatrix}1\\-1\end{Bmatrix} + (e_n(1-2\nu_n-\beta_{ml}x_3)\right.$$
$$\left.\left. - f_n\beta_{ml})\begin{Bmatrix}1\\-1\end{Bmatrix}\right)e^{\beta_{ml}x_3}\right]\begin{Bmatrix}\alpha_l\sin\alpha_m x_1\sin\alpha_l x_2\\ \alpha_m\cos\alpha_m x_1\cos\alpha_l x_2\end{Bmatrix}.$$

Aside from their use here, these eigenfunctions may be combined to represent any periodic shear loading of a layered elastic half-space. Last we give the elements of the *transfer matrix*, $\mathbf{T}_n^f$, for the *friction problem*:

$$\mathbf{T}_n^f = \begin{pmatrix}\mathbf{T}_n' & | & \mathbf{O}^T\\ \text{---} & + & \text{---}\\ \mathbf{O} & | & \mathbf{T}_n\end{pmatrix},$$

wherein $\mathbf{T}_n$ is as previously, $\mathbf{O}$ is a 4×2 matrix of zeros and $\mathbf{O}^T$ its transpose, and

$$\mathbf{T}_n' = \left(\frac{t'_{qs}(1-\nu_{n+1})}{2\mu_{n+1}(1-\nu_n)}\right),$$

where $t'_{qs}(q,s=1,2)$ are given by:

$$t'_{11} = t'_{22} = \mu_{n+1} + \mu_n,$$
$$t'_{12} = -\bar{\mu}_n e^{2\beta_{ml}D_n}, \quad t'_{21} = t'_{12}(-D).$$

Again the check case $\mu_{n+1} = \mu_n$, $\nu_{n+1} = \nu_n$ reduces $\mathbf{T}_n^f$ to the unit matrix.